small NANO MICRO

Field-Effect Transistors

N-Doped Graphene Field-Effect Transistors with Enhanced Electron Mobility and Air-Stability

*Wentao Xu, Tae-Seok Lim, Hong-Kyu Seo, Sung-Yong Min, Himchan Cho, Min-Ho Park, Young-Hoon Kim, and Tae-Woo Lee**

Although graphene can be easily p-doped by various adsorbates, developing stable n-doped graphene that is very useful for practical device applications is a difficult challenge. We investigated the doping effect of solution-processed (4-(1,3-dimethyl-2,3-dihydro-1H-benzoimidazol-2-yl)phenyl)dimethylamine (N-DMBI) on chemical-vapor-deposited (CVD) graphene. Strong n-type doping is confirmed by Raman spectroscopy and the electrical transport characteristics of graphene field-effect transistors. The strong n-type doping effect shifts the Dirac point to around –140 V. Appropriate annealing at a low temperature of 80 °C enables an enhanced electron mobility of 1150 $cm^2 V^{-1} s^{-1}$. The work function and its uniformity on a large scale (1.2 mm × 1.2 mm) of the doped surface are evaluated using ultraviolet photoelectron spectroscopy and Kelvin probe mapping. Stable electrical properties are observed in a device aged in air for more than one month.

1. Introduction

Graphene has superior electronic, physical and chemical properties, such as high carrier mobility at room temperature (>250 000 $cm^2 V^{-1} s^{-1}$), superior thermal conductivity (3000–5000 $W m^{-1} K^{-1}$), extremely high modulus (≈1 TPa) and high transparency to incident light over a broad wavelength range.[1–7] However, graphene has no bandgap, and this is an impediment to its electronic applications. To overcome this disadvantage, several approaches have been applied to engineer a bandgap in graphene, including fabrication of graphene nanoribbons,[8–15] nanomesh,[16,17] and doping of the graphene lattice.[18–21] P-type graphene channel can be easily prepared under air and oxygen atmosphere,[22–24] but n-type semiconducting graphene is not; complementary circuits require both p-type and n-type transistors, so a method to fabricate stable n-type graphene is imperative for development of such circuits based on graphene.

Chemical doping is one of the most feasible methods to control the carrier type (thus the Dirac point) and concentration in graphene.[25,26] Chemical doping can be roughly divided into two categories:[18,25] (1) surface transfer doping, including adsorption of gas,[27] metal[28], metal derivatives[29–33] or organic molecules[34,35] to the graphene surface and (2) substitutional doping, by periodic heteroatoms in a graphene lattice.[25,36–38] The surface transfer doping is an purely chemical approach that generates a built-in perpendicular electric field to open a band gap in bilayer graphene.[25] Defects in the lattice are introduced during the substitutional doping process, and partially reduce the carrier mobility,[25] while adsorption of organic molecular layers on graphene does not deteriorate the carrier mobility but shifts the position of the Dirac points of graphene.[22]

The presence of a chemical dopant layer on top of graphene induces a perpendicular electric field in a way similar to that which occurs when applying a gate voltage.[21] The type (i.e. electron or hole) and concentration of carriers can

Dr. W. Xu,[+] T.-S. Lim,[+] H.-K. Seo, S.-Y. Min, H. Cho, M.-H. Park, Y.-H. Kim, Prof. T.-W. Lee
Department of Materials Science and Engineering
Pohang University of Science and Technology (POSTECH)
Pohang, Gyungbuk 790-784, Republic of Korea
E-mail: twlee@postech.ac.kr
[+]W. Xu and T.-S. Lim contributed equally to this work.

DOI: 10.1002/smll.201303768

be controlled by the introduction of metals or molecules onto the graphene surface.[22] Currently, p-type molecular doping has been frequently investigated using strong acceptors, and a wide range of materials has been tested as p-type dopants. However, compared to highly doped p-channel organic semiconductors, there is few n-channel materials with high performance, air-stability, and solution processibility.[22,39] This is attributed to the vulnerability of electrons to trapping by ambient oxidants, such as O_2 and H_2O.[23,24] The design of n-type dopant is challenging owing to the requirement for high-lying highest occupied molecular orbital (HOMO) levels in the dopant because high HOMO levels are unstable against O_2.[40] Therefore, developing air-stable n-type properties in graphene is a difficult challenge.

(4-(1,3-dimethyl-2,3-dihydro-1*H*-benzoimidazol-2-yl) phenyl)dimethylamine (N-DMBI) is an effective n-type dopant of the PCBM channel in organic field-effect transistors (OFETs).[41] The dopant is inactive but can be activated by thermal annealing in an inert atmosphere after film formation has completed. Annealing causes the N-DMBI molecules to release a hydrogen atom and become radicals. The strong doping effect comes from the inner molecular highly-energetic neutral radicals, which have an extremely high singly-occupied molecular orbital level of 2.36 eV below vacuum; this level is shallow enough to donate electrons. This radical type of dopant is much stronger than conventional n-dopants, whose lone pair of electrons in nitrogen plays an dominant role in electron donation.[22] N-DMBI is also solution-processible, and offers significant improvement in the air-stability of [6,6]-phenyl C61 butyric acid methyl ester (PCBM) OFETs.[42–44] These superior properties of N-DMBI make it a promising candidate dopant with solution processibility for fabricating n-channel graphene-based electronic devices with high electron mobility and air-stability. Therefore, a study of the possible doping effect of N-DMBI on graphene would be very valuable.

In this work, we investigated the doping effect of solution-processed N-DMBI on graphene. The doping effect was confirmed by Raman spectroscopy, ultraviolet photoelectron spectroscopy (UPS) and Kelvin probe measurements. FETs with as-transferred and doped graphene as an active channel were fabricated to study the electrical transport characteristics and air-stability. We achieved an enhanced electron mobility of 1150 $cm^2\ V^{-1}\ s^{-1}$ utilizing the n-doped CVD-grown graphene as an active layer.

2. Results and Discussion

Raman spectroscopy is a powerful tool for monitoring the number of layers, disorder and doping of graphene.[45] Typical G and 2D peaks in Raman spectra of the as-transferred graphene differs from those of graphene doped with N-DMBI (**Figure 1**a). The as-transferred graphene showed a G peak at 1601 cm^{-1} and a 2D peak at 2687 cm^{-1}.

To identify the doping effect, G peak positions were plotted with respect to annealing temperatures, as shown in Figure 1b. The G peaks of the doped graphene all showed downshifts as compared with the as-transferred graphene.

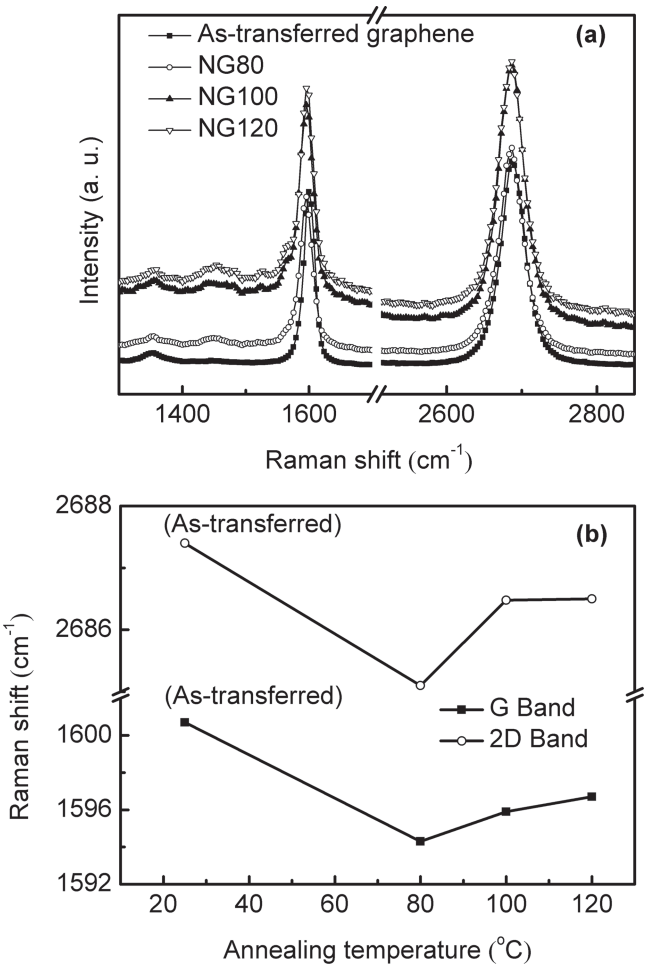

Figure 1. (a) Raman spectra of the as-transferred graphene and N-DMBI-doped graphene annealed at 80 °C (NG80), 100 °C (NG100) and 120 °C (NG120); (b) G and 2D peak shift of the as-transferred graphene and N-DMBI-doped graphene annealed at 80 °C, 100 °C and 120 °C.

The downshift of the G band by n-type doping is also found in previous reports.[46–48] The Raman G peak is sensitive to chemical doping; an empirical rule can be used to determine the doping type for surface transfer doping of graphene:[25,46] for n-type doped graphene, or adsorption of molecules with electron-donating groups, the G band downshifts and stiffens; for p-type doped graphene, or adsorption of electron-withdrawing molecules, it up-shifts and softens.[25] In comparison to the as-transferred graphene, the 2D band gradually down-shifted to 2682 cm^{-1} with increased annealing temperatures, therefore the rule indicates that adsorption of the electron-donating N-DMBI on the graphene results in n-type doped graphene. The electron-doped graphene can be simply identified by Raman spectroscopy based on the down-shift of the 2D and G bands.[25] Similar down-shifts of the G band by n-doping have also been reported in single-wall nanotubes and has been attributed to electronics effects.[49,50] These rules are different from those of substitutional doping, in which both nitrogen and boron substitutionally-doped graphene have an up-shift of the G band.[51] Among the annealed samples, N-DMBI-doped graphene that was annealed at 80 ºC (NG80) exhibited the

small NANO MICRO

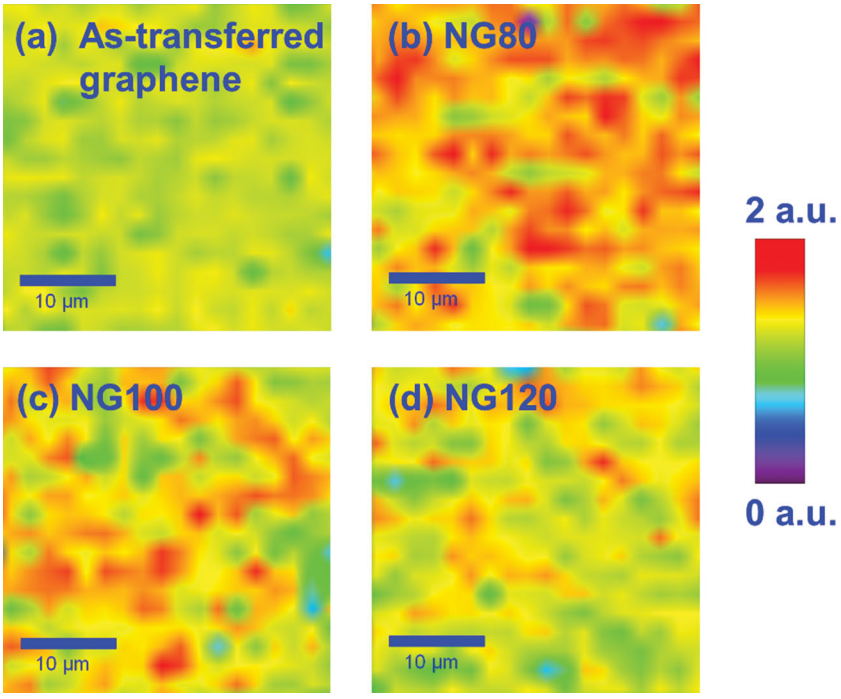

Figure 2. Mapping of 2D/G intensity ratio of (a) as-transferred graphene and N-DMBI-doped graphene annealed at (b) 80 °C, (c) 100 °C, (d) 120 °C.

most significant down shift of G band, and therefore had the strongest doping.

The doping condition cannot be simply determined by analyzing the intensity ratio of Raman D and G peaks (I_D/I_G) as well as the intensity ratio of Raman 2D and G peaks (I_{2D}/I_G), which are derived from the Raman spectra at discrete spots. Raman spectral mapping can be used to avoid this problem. The comparison of different n-doped graphene with as-transferred graphene is convincing to show the most homogeneous doping of NG80 when the Raman response is monitored on a large scale.[18] Aromatic ring structures can firmly attach on the surface of graphene by π–π interaction as a dopant. On a 40 μm × 40 μm scale, I_{2D}/I_G was increased after molecular doping (**Figure 2**). This is because the n-type dopant compensated the p-type doping effect in CVD-grown graphene stemming from PMMA residue and adsorbed O_2 and moisture on the surface.[52]

Mapped on a on a 40 μm × 40 μm scale, I_D/I_G was slightly higher in undoped graphene (Figure S1), but the value both <0.1, suggesting that high quality graphene with a quite limited number of defects remained after the doping process.[25] This is superior to the substitutional doping process, which usually introduces numerous defects into the graphene.

UPS spectra (**Figure 3**) of as-transferred graphene and NG80 were taken to calculate the work function ϕ,[53,54]

$$\phi = h\nu - E_{cutoff} + E_{Fermi} \quad (1)$$

where $h\nu$ = 21.2 eV is the photon energy of the UPS light source (helium I irradiation) and E_{cutoff}, and E_{Fermi} are secondary electron cutoff level and the Fermi level, respectively. Using this equation, the UPS spectra (Figure 3) indicate that ϕ = 4.01 eV for as-transferred graphene and 3.80 eV for NG80.

The work function on a large scale (1.2 mm × 1.2 mm) was mapped using a Kelvin probe[55] (**Figure 4**). The work function difference of ≈0.2 eV between NG80 and as-transferred graphene is consistent with UPS results. The negligible fluctuations of work function (<0.01 eV) are ±0.003 V for NG80, ±0.009 V for NG100 and ±0.005 eV for NG120, indicative of high-quality, uniformly-doped surfaces. NG100 and NG120 showed slightly higher work functions than did NG80 (Figure S2); these differences indicate that the doping effect is weaker in NG100 and NG120 than in NG80.

FETs (**Figure 5**) were fabricated to evaluate the electrical transport properties of the doped graphene.[56–60] The FET (Figure 5a) consisted of N-DMBI doped graphene ribbons

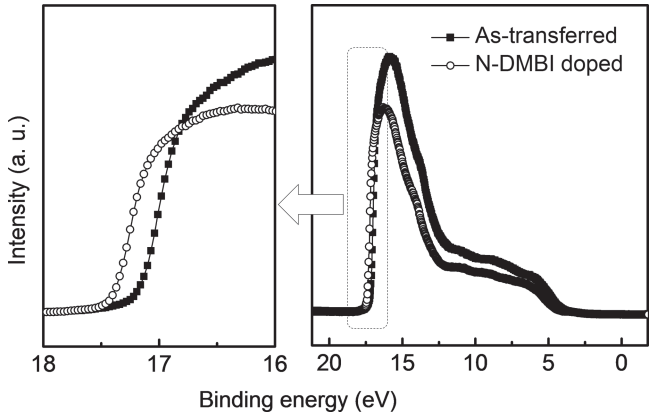

Figure 3. UPS spectra of as-transferred graphene and N-DMBI-doped graphene annealed at 80 °C.

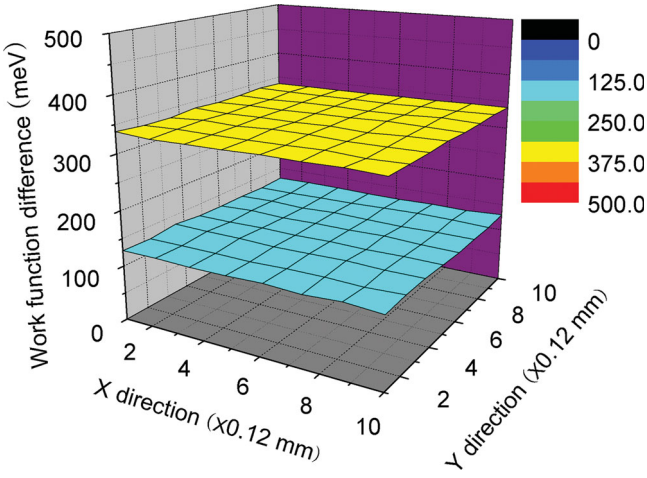

Figure 4. Kelvin probe mapping at a 1.2 mm × 1.2 mm scale of as-transferred graphene (yellow) and N-DMBI-doped graphene annealed at 80 °C (blue).

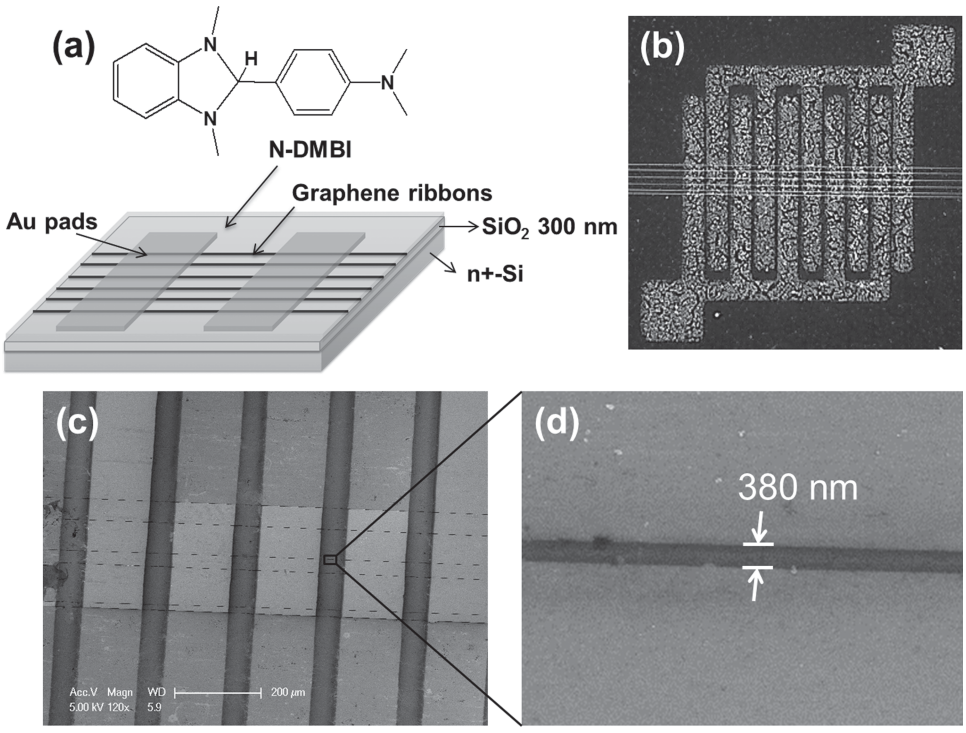

Figure 5. (a) Schematic of N-DMBI-doped graphene transistor, (b) OM images of the top electrodes and with PVK nanowires, SEM images of (c) channel regions of the a FET device and (d) specific graphene patterns in the channel area.

(GRs), top electrodes and a 300 nm-SiO_2/n+Si substrate. PVK nanowires with diameter of ≈430 nm (Figure 5b) was used as an etch mask to pattern the graphene sheet, which were then removed to leave GR with width of ≈380 nm (Figure 5c,d). Judging from optical microscope (Figure 5b) and scanning electron microscope (SEM) (Figure 5c,d), the graphene nanoribbons was really continuous while they appeared discontinuous in the SEM image (Figure 5c) due to the miscroscopic artifact.

Electrical characteristics of n-type and p-type doped graphene FET devices were measured.[61,62] The transfer and output characteristics of the graphene FETs were affected by doping (**Figure 6**). The FETs with as-transferred graphene showed a large positive Dirac point at 100 V, suggesting p-type behavior in air. This behavior is due to residual PMMA on the graphene surface, and to moisture, oxygen, or defects introduced in the graphene during device fabrication. PMMA residue on CVD graphene make a significant influence on p-type chemical doping.[63,64] Typically, the minimum conductivity (or maximum resistivity) point or the Dirac point of pristine undoped graphene is expected to be located around zero gate voltage,[23,24,64] and the point shifted toward positive gate voltage as a consequence of p-type doping of graphene, or to negative gate voltage as a consequence of n-type doping. This is in consistence with several comparable works.[23,24] The Dirac point shifted towards zero gate voltage to ≈10 V after annealing at 200 °C for 30 min, suggesting partial removal of the adsorbates (Figure S3). The graphene FET-NG80 displays a clear n-type behavior with the Dirac point at the negative gate voltage of –140 V; this result confirms that the doping of graphene was n-type. Due to sensitive GR edges,[19,26] the change in Dirac voltage of the GR based devices is more significant than that in work function (0.2 eV) as measured from graphene sheets. The N-DMBI doping on the graphene channel resulted in remarkably strong n-type FETs. The carrier mobility μ can be calculated as

$$\mu = \frac{L}{W} C_g V_{sd} \frac{\Delta I_{sd}}{\Delta V_g} \quad (2)$$

where C_g is the gate capacitance per unit area; L = 50 μm is channel length, W = 380 nm is channel width (GNR width); V_{sd} source-drain voltage (=1 mV in our experiment). FET-NG80 exhibits significantly enhanced electron mobility ≈1150 $cm^2\ V^{-1}\ s^{-1}$ and reduced hole mobility ≈85 $cm^2\ V^{-1}\ s^{-1}$ as compared with the FET with as-etched GR, which has a hole mobility ≈1450 $cm^2\ V^{-1}\ s^{-1}$ and electron mobility ≈300 $cm^2\ V^{-1}\ s^{-1}$. Increase in electron mobility and reduction in hole mobility in graphene FETs were also consistent with a recent report on chemical transfer doping.[22,65] For the FET with annealed undoped GR, the electron mobility ≈450 $cm^2\ V^{-1}\ s^{-1}$ and hole mobility ≈1050 $cm^2\ V^{-1}\ s^{-1}$ is in between those of the as-transferred graphene and NG80.

Increase of mobility with adsorbed n-type dopant was also reported recently in a bilayer graphene-based device.[22] The enhanced electron mobility in our device (1150 $cm^2\ V^{-1}\ s^{-1}$) is twice as large as that of the most recently reported graphene-based device (≈550 $cm^2\ V^{-1}\ s^{-1}$), implying that our graphene films were high quality and were doped effectively with fewer defects. This is different from the substitutional doped graphene device, in which n-doped graphene behaves like an n-type doped semiconductor with lower conductivity and lower mobility (≈200–450 $cm^2\ V^{-1}\ s^{-1}$).[25] The calculated electron mobility was higher in FET-NG80 than in devices fabricated using NG100 and NG120. Appropriate thermal annealing could

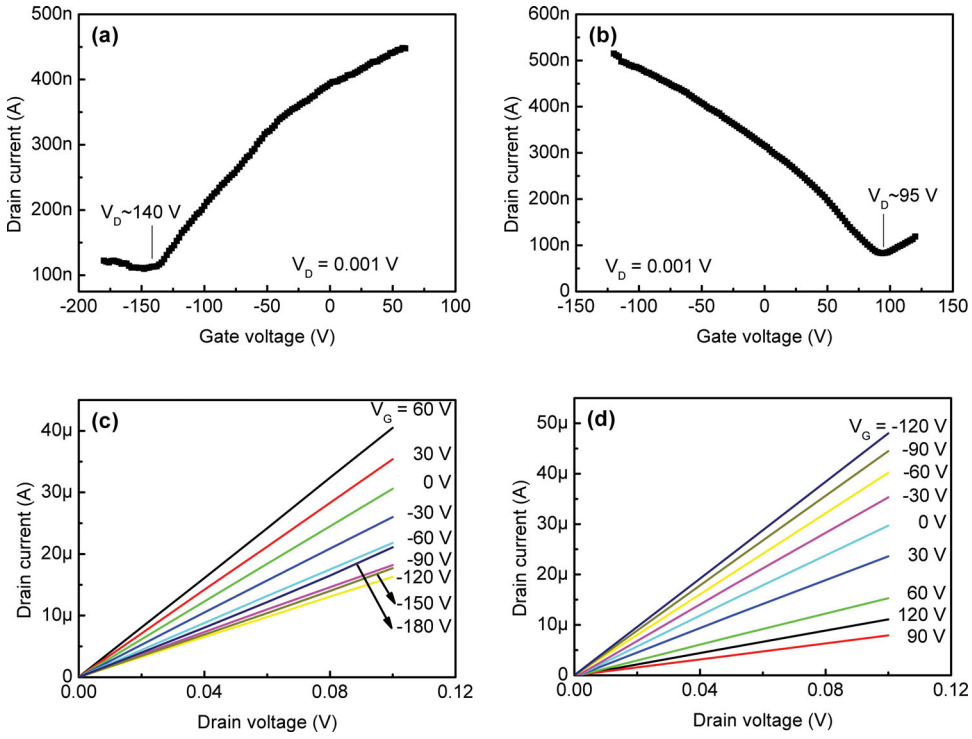

Figure 6. Transfer curves of graphene FETs with (a) N-DMBI-doped graphene annealed at 80 °C and (b) as-transferred graphene as a conductive channel; Output curves of field-effect transistors with (c) N-DMBI-doped graphene annealed at 80 °C and (d) as-transferred graphene as a conductive channel.

activate N-DMBI to release an H atom and form an N-DMBI radical.[41] This inner molecular highly energetic neutral radical posseses a singly occupied molecualr orbital of 2.36 eV below vacuum,[42] which is shallow enough to donate electrons as a strong n-dopant. This radical-type dopant is much stronger than conventional ones with the lone pairs of electrons as donating sites. However, N-DMBI tends to severely aggregate into larger particles as annealing temperature increased to 100 °C and 120 °C (OM images in Figure S4). This reduces the contact area between the N-DMBI and the underlying graphene. N(1s) responses in the XPS spectra (**Figures 7**a) were mainly restricted within 400.0 eV and 401.5 eV in N(1s), indicative of pyrrolic N.[18,31–33] Further separation of the peaks (Figure 7b) distinguished the interactions between N-DMBI and graphene (N-G) and the intermolecular interaction between N-DMBI molecules (N-N). Increased annealing temperatures reduces N-G interaction and enhanced the N-N interaction, which is consistent with the more severe aggregation at higher temperatures in OM. According to the ratio of N-G N(1s) response and the C(1s) response of as-transferred graphene, the real doping values were calculated as 12.5%, 9.1% and 6.7% for NG80, NG100 and NG120, respectively.

Obtaining a graphene FET with air-stability against oxygen and atmospheric moisture is one of the most important challenges in graphene electronics.[22,39] Aged under ambient air condition with himidity of 40–50%, the electrical properties of our graphene FETs stabilized after 24 h (**Figure 8**a). The Dirac point and electron mobility stabilized at around –110 V after 24 h, and did not show significant shift in one month (Figure 8b). The result indicates that the n-type doped graphene was stable under these ambient conditions. During the initial 24 h, the shift in Dirac point and degradation in mobility was due to the adsorption of various adsorbates in the air, such as moisture and gaseous molecules. After the amount of adsorbates saturated on the device surface during the first day, further adsorption would be relatively difficult and hence the electrical properties became relatively stable during the following one

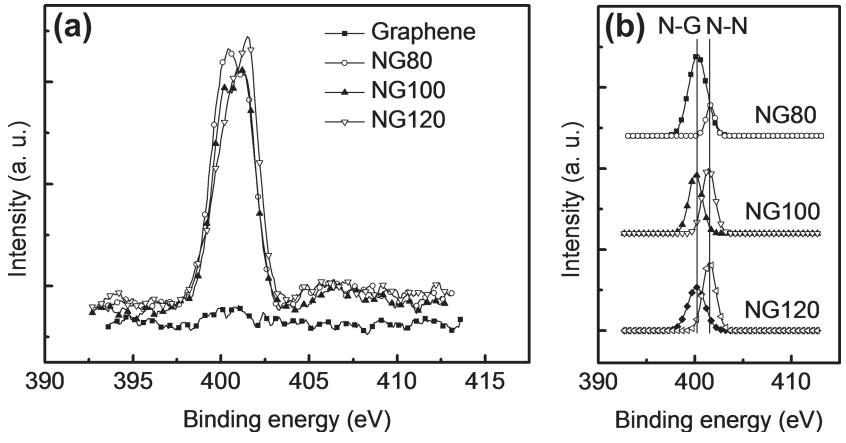

Figure 7. (a) N(1s) responses in XPS analysis of as-transferred graphene NG80, NG100 and NG120. (b) Peak separation of N(1s) responses of NG80, NG100 and NG120 and the comparison of the contribution of the interactions between N-DMBI and graphene (N-G) and the intermolacular interaction between N-DMBI molecules (N-N).

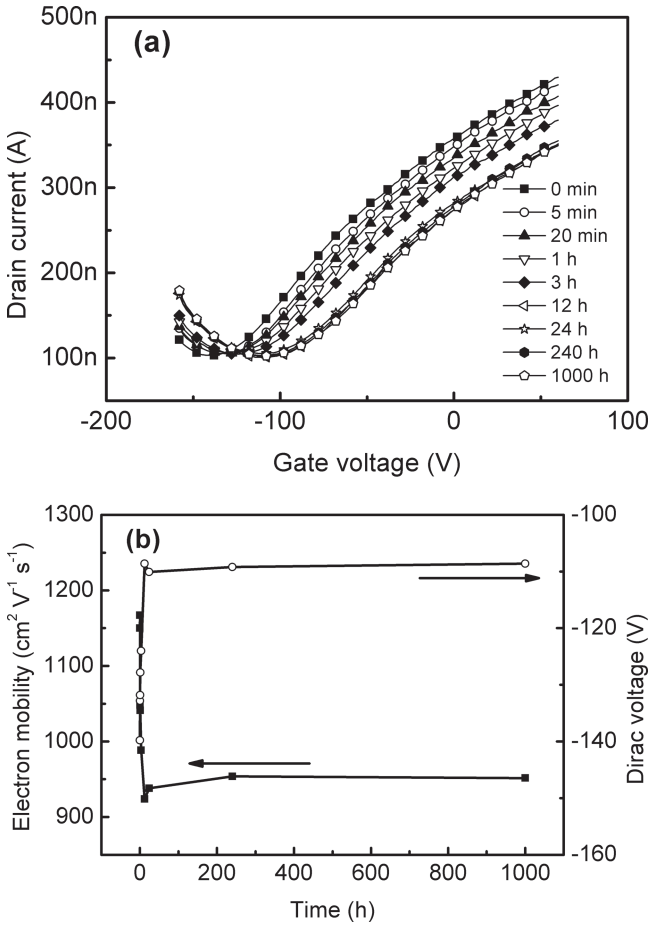

Figure 8. (a) Transfer curves of an N-DMBI-doped graphene FET at different exposure time to air; (b) mobility and Dirac voltage of the same graphene FET at different exposure time to air.

month. Mobile electrons generated by n-type doping are located abundantly in the bulk active layer or in the channel region, and can compensate for the trapped electrons to a significant degree, thereby maintaining the n-type dominated electrical performance of the devices in air.[22]

3. Conclusion

We demonstrated stable chemical doping using solution-processed N-DMBI on CVD-grown graphene. A strong n-doping effect was confirmed by Raman spectroscopy and a far negative Dirac-point shift in FET-characteristics. The FETs fabricated using this graphene had electron mobility > 1000 $cm^2\ V^{-1}\ s^{-1}$, and had stable electrical characteristics in air for more than one month. UPS and Kelvin probe analysis revealed a reduced work function, which was uniform on a large scale.

4. Experimental Section

Materials Synthesis and Device Fabrication: N-DMBI was synthesized according to the literature.[66] It was purified by recrystallization from methanol by addition of water, and filtered through a Buchner funnel. Graphene was grown on a copper foil (99.8% purity, 25 μm thick, Alfa Aesar) using chemical vapor deposition in a quartz tube at 1000 °C, with a mixed gas flow of H_2 15 sccm and CH_4 25 sccm. The synthesized graphene sheet was transferred onto a 300-nm-thick SiO_2/n+Si substrate. The thickness of the graphene was about 1.2 nm as measured at the edge by atomic force microscopy (AFM), which is in between single- and double-layer graphene on SiO_2 substrates (Figure S5).[15] 60-nm/Ti 3-nm source-drain electrodes were patterned on the graphene sheet through shadow masks (Figure 5a).[21] Aligned polyvinyl carbazole (PVK) nanowires (NWs) were deposited using electrostatic hydrodynamic printing (Figure 5b). O_2 plasma (BCS5004, SNTEK) was then applied to selectively etch away the unprotected graphene region to produce submicron ribbons (Figure 5c,d). The etching time was 10 s at a power level of 30 W and O_2 flow of 20 sccm. The protective NWs were removed by sonication in chloroform for 30 s, and then the graphene ribbons were blown dry. N-DMBI (0.5 w.t.% in chlorobenzene) was then spin-coated under the ambient air condition to form a doping layer. To examine the effect of thermal treatment, graphene devices were annealed at 80 °C, 100 °C or 120 °C for 30 min.

Measurements: SEM imaging was performed on a JEOL-6500 field-emission microscope. Raman spectroscopy was obtained using a confocal Raman microscope (Alpha 300R, Witec). UPS was performed using an Escalab 220IXL. Kelvin probe mapping was performed using a Scanning Kelvin probe (SKP5050, Kelvin Probe Technology, Ltd., Wick, UK), which is a state-of-the-art device that measures surface electrical potential without actually contacting the sample.[53] The electrical transport properties were tested using a probe station in an N_2-filled glove box. The IV data were collected using a Keithley 4200 semiconductor parameter analyzer.

Supporting Information

Supporting Information is available from the Wiley Online Library or from the author.

Acknowledgements

This research was supported by the Pioneer Research Center Program through the National Research Foundation (NRF) of Korea funded by the Ministry of Science, ICT & Future Planning (2012-0009460) and supported by Basic Science Research Program through the National Research Foundation of Korea funded by the Ministry of Education (NRF-2013R1A1A2012660).

[1] K. S. Novoselov, A. K. Geim, S. V. Morozov, D. Jiang, Y. Zhang, S. V. Dubonos, I. V. Grigorieva, A. A. Firsov, *Science* **2004**, *306*, 666.
[2] F. Schwierz, *Nature* **2011**, *472*, 41.
[3] L. Ma, J. Wang, F. Ding, *ChemPhysChem* **2013**, *14*, 47.
[4] T.-H. Han, Y. Lee, M.-R. Choi, S.-H. Woo, S.-H. Bae, B. H. Hong, J.-H. Ahn, T.-W. Lee, *Nat. Photonics* **2012**, *6*, 105.
[5] S.-J. Byun, H. Lim, G.-Y. Shin, T.-H. Han, S. H. Oh, J.-H. Ahn, H. C. Choi, T.-W. Lee, *J. Phys. Chem. Lett.* **2011**, *2*, 493.

[6] S. Bae, H. Kim, Y. Lee, X. Xu, J.-S. Park, Y. Zheng, J. Balakrishnan, T. Lei, H. R. Kim, Y. I. Song, Y.-J. Kim, K. S. Kim, B. Özyilmaz, J.-H. Ahn, B. H. Hong, S. Iijima, *Nat. Nanotechnol.* **2010**, *5*, 574.
[7] Z. Yan, J. Lin, Z. Peng, Z. Sun, Y. Zhu, L. Li, C. Xiang, E. L. Samuel, C. Kittrell, J. M. Tour, *ACS Nano* **2012**, *6*, 9110.
[8] M. Y. Han, B. Özyilmaz, Y. Zhang, P. Kim, *Phys. Rev. Lett.* **2007**, *98*, 206805.
[9] T. Kato, R. Hatakeyama, *Nat. Nanotechnol.* **2012**, *7*, 651.
[10] J. Bai, X. Duan, Y. Huang, *Nano Lett.* **2009**, *9*, 2083.
[11] G. Xie, Z. Shi, R. Yang, D. Liu, W. Yang, M. Cheng, D. Wang, D. Shi, G. Zhang, *Nano Lett.* **2012**, *12*, 4642.
[12] L. Liao, J. Bai, Y.-C. Lin, Y. Qu, Y. Huang, X. Duan, *Adv. Mater.* **2010**, *22*, 1941.
[13] M. Sprinkle, M. Ruan, Y. Hu, J. Hankinson, M. Rubio-Roy, B. Zhang, X. Wu, C. Berger, W. A. de Heer, *Nat. Nanotechnol.* **2010**, *5*, 727.
[14] A. Sinitskii, J. M. Tour, *Appl. Phys. Lett.* **2012**, *100*, 103106.
[15] X. Wang, Y. Ouyang, X. Li, H. Wang, J. Guo, H. Dai, *Phys. Rev. Lett.* **2008**, *100*, 206803.
[16] L. Liu, Y. Zhang, W. Wang, C. Gu, X. Bai, E. Wang, *Adv. Mater.* **2011**, *23*, 1246.
[17] J. Bai, X. Zhong, S. Jiang, Y. Huang, X. Duan, *Nat. Nanotechnol.* **2010**, *5*, 190.
[18] H. Wang, T. Maiyalagan, X. Wang, *ACS Catalysis* **2012**, *2*, 781.
[19] B. Guo, L. Fang, B. Zhang, J. R. Gong, *Insciences J.* **2011**, *1*, 80.
[20] B. Guo, Q. Liu, E. Chen, H. Zhu, L. Fang, J. R. Gong, *Nano Lett.* **2010**, *10*, 4975.
[21] J. Park, S. B. Jo, Y.-J. Yu, Y. Kim, J. W. Yang, W. H. Lee, H. H. Kim, B. H. Hong, P. Kim, K. Cho, K. S. Kim, *Adv. Mater.* **2012**, *24*, 407.
[22] S. Some, J. Kim, L. Lee, A. Kulkarni, Y. Yoon, S. M. Lee, T. Kim, H. Lee, *Adv. Mater.* **2012**, *24*, 5481.
[23] Z. Cheng, Q. Zhou, C. Wang, Q. Li, C. Wang, Y. Fang, *Nano Lett.* **2011**, *11*, 767.
[24] Y.-C. Lin, C.-C. Lu, C.-H. Yeh, C. Jin, K. Suenaga, P.-W. Chiu, *Nano Lett.* **2012**, *12*, 414.
[25] H. Liu, Y. Liu, D. Zhu, *J. Mater. Chem.* **2011**, *21*, 3335.
[26] X. Wang, X. Li, L. Zhang, Y. Yoon, P. K. Weber, H. Wang, J. Guo, H. Dai, *Science* **2010**, *324*, 768.
[27] F. Schedin, A. K. Geim, S. V. Morozov, E. W. Hill, P. Blake, M. I. Katsnelson, K. S. Novoselov, *Nat. Mater.* **2007**, *6*, 652.
[28] G. Giovannetti, P. A. Khomyakov, G. Brocks, V. M. Karpan, J. van der Brink, P. J. Kelly, *Phys. Rev. Lett.* **2008**, *101*, 026803.
[29] K. C. Kwon, K. S. Choi, S. Y. Kim, *Adv. Funct. Mater.* **2012**, *22*, 4724.
[30] K. C. Kwon, K. S. Choi, B. J. Kim, J.-L. Lee, S. Y. Kim, *J. Phys. Chem. C* **2012**, *116*, 26586.
[31] X. Wang, X. Cao, L. Bourgeois, H. Guan, S. Chen, Y. Zhong, D.-M. Tang, H. Li, T. Zhai, L. Li, Y. Bando, D. Golberg, *Adv. Funct. Mater.* **2012**, *22*, 2682.
[32] X. Wang, W. Tian, D. Liu, C. Zhi, Y. Bando, D. Golberg, *Nano Energy* **2013**, *2*, 257.
[33] C. Nethravathi, C. R. Rajamathi, M. Rajamathi, U. K. Gautam, X. Wang, D. Golberg, Y. Bando, *ACS Appl. Mater. Interfaces* **2013**, *5*, 2708.
[34] W. Chen, S. Chen, D. C. Qi, X. Y. Gao, A. T. S. Wee, *J. Am. Chem. Soc.* **2007**, *129*, 10418.
[35] J. O. Hwang, J. S. Park, D. S. Choi, J. Y. Kim, S. H. Lee, K. E. Lee, Y.-H. Kim, M. H. Song, S. Yoo, S. O. Kim, *ACS Nano* **2012**, *6*, 159.
[36] L. Lai, J. R. Potts, D. Zhan, L. Wang, C. K. Poh, C. Tang, H. Gong, Z. Shen, J. Lin, R. S. Ruoff, *Energy Environ. Sci.* **2012**, *5*, 7936.
[37] L. L. Zhang, X. Zhao, H. Ji, M. D. Stoller, L. Lai, S. Murali, S. Mcdonnell, B. Cleveger, R. M. Wallance, R. S. Ruoff, *Energy Environ. Sci.* **2012**, *5*, 9618.
[38] Z. Jin, J. Yao, C. Kittrell, J. M. Tour, *ACS Nano* **2011**, *5*, 4112.
[39] P.-H. Ho, Y.-C. Yeh, D.-Y. Wang, S.-S. Li, H.-A. Chen, Y.-H. Chung, C.-C. Lin, W.-H. Wang, C.-W. Chen, *ACS Nano* **2012**, *6*, 6215.
[40] K. Walzer, B. Maennig, M. Pfeiffer, K. Leo, *Chem. Rev.* **2007**, *107*, 1233.
[41] P. Wei, J. H. Oh, G. Dong, Z. Bao, *J. Am. Chem. Soc.* **2010**, *132*, 8852.
[42] M. Lu, H. T. Nicolai, G.-J. A. H. Wetzelaer, P. W. M. Blom, *Appl. Phys. Lett.* **2011**, *99*, 173302.
[43] J. H. Oh, P. Wei, Z. Bao, *Appl. Phys. Lett.* **2010**, *97*, 243305.
[44] M. P. Ramuz, M. Vosgueritchian, P. Wei, C. Wang, Y. Gao, Y. Wu, Y. Chen, Z. Bao, *ACS Nano* **2012**, *6*, 10384.
[45] A. C. Ferrani, J. C. Meyer, V. Scardaci, C. Casiraghi, M. Lazzeri, F. Mauri, S. Piscanec, D. Jiang, K. S. Novoselov, S. Roth, A. K. Geim, *Phys. Rev. Lett.* **2006**, *97*, 187401.
[46] X. Dong, D. Fu, W. Fang, Y. Shi, P. Chen, L.-J. Li, *Small* **2009**, *5*, 1422.
[47] R. Lv, Q. Li, A. R. Botello-Méndez, T. Hayashi, B. Wang, A. Berkdemir, Q. Hao, A. L. Elías, R. Cruz-Silva, H. R. Gutiérrez, Y. A. Kim, H. Muramatsu, J. Zhu, M. Endo, H. Terrones, J.-C. Charlier, M. Pan, M. Terrones, *Sci. Rep.* **2013**, *2*, 586.
[48] B. Das, R. Voggu, C. S. Rout, C. N. R. Rao, *Chem. Commun.* **2008**, *2008*, 5155.
[49] H.-J. Shin, S. M. Kim, S.-M. Yoon, A. Benayad, K. K. Kim, S. J. Kim, H. K. Park, J.-Y. Choi, Y. H. Lee, *J. Am. Chem. Soc.* **2008**, *130*, 2062.
[50] R. Voggu, C. S. Rout, A. D. Franklin, T. S. Fisher, C. N. R. Rao, *J. Phys. Chem. C* **2008**, *112*, 13053.
[51] L. S. Panchakarla, K. S. Subrahmanyam, S. K. Saha, A. Govindaraj, H. R. Krishnamurthy, U. V. Waghmare, C. N. R. Rao, *Adv. Mater.* **2009**, *21*, 4726.
[52] P. Wei, N. Liu, H. R. Lee, E. Adijanto, L. Ci, B. D. Naab, J. Q. Zhong, J. Park, W. Chen, Y. Cui, Z. Bao, *Nano Lett.* **2013**, *13*, 1890.
[53] A. Cahen, A. Kahn, *Adv. Mater.* **2003**, *15*, 271.
[54] W. Xu, S.-W. Rhee, *Org. Electron.* **2010**, *11*, 996.
[55] B. J. Gow, J. L. Cheng, I. D. Baikie, Ø. G. Martinsen, M. Zhao, S. Smith, A. C. Ahn, *Evid. Based Complement Alternat. Med.* **2012**, *2012*, 632838.
[56] B. J. Kim, S.-K. Lee, M. S. Kang, J.-H. Ahn, J. H. Cho, *ACS Nano* **2012**, *6*, 8646.
[57] S.-K. Lee, B. J. Kim, H. Jang, S. C. Yoon, C. Lee, B. H. Hong, J. A. Rogers, J. H. Cho, J.-H. Ahn, *Nano Lett.* **2011**, *11*, 4642.
[58] J. Lee, L. Tao, Y. Hao, R. S. Ruoff, D. Akinwande, *Appl. Phys. Lett.* **2012**, *100*, 152104.
[59] S.-Y. Chen, P.-H. Ho, R.-J. Shiue, C.-W. Chen, W.-H. Wang, *Nano Lett.* **2012**, *12*, 964.
[60] J. Lee, L. Tao, K. N. Parrish, Y. Hao, R. S. Ruoff, D. Akinwande, *Appl. Phys. Lett.* **2012**, *101*, 252109.
[61] F. Schwierz, *Nat. Nanotechnol.* **2010**, *5*, 487.
[62] I. Martin-Fernandez, D. Wang, Y. Zhang, *Nano Lett.* **2012**, *12*, 6175.
[63] A. Pirkle, J. Chan, A. Venugopal, D. Hinojos, C. W. Magnuson, S. McDonnell, L. Colombo, E. M. Vogel, R. S. Ruoff, R. M. Wallace, *Appl. Phys. Lett.* **2011**, *99*, 122108.
[64] J. W. Suk, W. H. Lee, J. Lee, H. Chou, R. D. Piner, Y. Hao, D. Akinwande, R. S. Ruoff, *Nano Lett.* **2013**, *13*, 1462.
[65] Z. Yan, J. Yao, Z. Sun, Y. Zhu, J. M. Tour, *Small* **2012**, *8*, 59.
[66] X.-Q. Zhu, M.-T. Zhang, A. Yu, C.-H. Wang, J.-P. Cheng, *J. Am. Chem. Soc.* **2008**, *130*, 2501.

Received: December 7, 2013
Revised: January 9, 2014
Published online: February 24, 2014